#### **Research Article**

Zhengyi Fu, Sansan Ding\*, Aiqin Tian, Dawei Chen, Xu Chen, Huaqiang Lin, Zhongwen Li, Xiaohong Sun, Xiangjian Meng, and Wei Zhou\*

# Effects of C and heat treatment on microstructure, mechanical, and tribo-corrosion properties of VAITiMoSi high-entropy alloy coating

https://doi.org/10.1515/rams-2024-0018 received December 08, 2023; accepted April 10, 2024

Abstract: High-entropy alloy (HEA) coatings have demonstrated great potential in anti-wear applications. To further improve the mechanical and tribo-corrosion properties of the HEA coatings, the VAlTiMoSi, (VAlTiMoSi)<sub>80</sub>C<sub>20</sub>, and (VAlTiMoSi)<sub>60</sub>C<sub>40</sub> coatings were successfully deposited by DC magnetron sputtering. The microstructure, mechanical, and tribo-corrosion properties of as-deposited and heattreated coatings were analyzed. All the as-deposited HEA coatings were BCC + amorphous phases. The thermal effect promoted the formation of intermetallic compounds, and the C inhibited the formation of Mo<sub>3</sub>Si and Ti<sub>5</sub>Si<sub>4</sub>. The hardness and elastic modulus of the heat-treated VAlTiMoSi coating were 20.1 and 294.0 GPa, respectively. The heattreated (VAlTiMoSi)<sub>60</sub>C<sub>40</sub> coating showed the lowest wear rate, namely  $5.2 \times 10^{-14} \,\mathrm{m}^3 \cdot \mathrm{Nm}^{-1}$ , and the best formation ability of passive film in 3.5 wt% NaCl solution.

**Keywords:** high-entropy carbides, mechanical performance, wear resistance, heat treatment, magnetron sputtering

Zhengyi Fu, Aiqin Tian, Dawei Chen, Xu Chen, Huaqiang Lin, Zhongwen Li, Xiaohong Sun, Xiangjian Meng: CRRC Qingdao Sifang Co., Ltd., Qingdao, 266111, China

#### 1 Introduction

The marine economy and resource exploration have gained significant attention in various countries. The ocean engineering equipment plays a momentous role in the ocean development. However, friction and corrosion in the seawater environment severely reduce the operating stability and service life of components [1]. Therefore, the protection of the sea-related components, such as ocean platforms, pumps, and lifting systems, come as a worldwide issue. The tribo-corrosion resistance coating coated on the component is an economical and effective fashion to improve the wear resistance and corrosion resistance. Nowadays, nitride and carbide coating are the main protective coatings for marine components [2,3]. However, cracking and peeling have not yet been properly resolved, and research bottlenecks began to appear for conventional protective coatings [4,5]. For this reason, a novel material system may inspire some unexpected achievement for the marine protective coatings.

High entropy alloy (HEA) coating has a great potential in structural design and performance modulation due to the unique lattice distortion, high entropy effect, cocktail effect, and sluggish effect. Therefore, quite a few material systems and structures are designed to fulfill the excellent tribo-corrosion resistance. For the corrosion resistance, it is suggested that the passive film derived from HEA coating has a low donor density and a high ability to inhibit ions adsorption [6]. The reduced point-defect density in the passive film also plays a decisive role in corrosion resistance [7]. Wang et al. [6] assessed the tribo-corrosion resistance of the (TiZrNbTaMo)C HEA coating in 3.5 wt% NaCl solution, impressively, the self-corrosion current density of the HEA coating was one order of magnitude lower than that of bare CP-Ti. For the wear resistance, the phase modification [8], elemental type/content [9], carbonization/

<sup>\*</sup> Corresponding author: Sansan Ding, CRRC Qingdao Sifang Co., Ltd., Qingdao, 266111, China, e-mail: sf-dingsansan@cqsf.com

<sup>\*</sup> Corresponding author: Wei Zhou, Key Laboratory of Traffic Safety on Track, Ministry of Education, School of Traffic & Transportation Engineering, Central South University, Changsha, 410083, China, e-mail: gszx\_zhouwei@csu.edu.cn

nitriding [10], heat treatment [11], etc., feature in enhancing the hardness of the coating and likewise contribute to reducing wear loss. Niu et al. [12] evaluated that the doping of carbon in HEA coating effectively made the structure dense, and higher content of C benefited in improving the tribo-corrosion resistance. In particular, the N-doped CrNbTiAlV coating obtained an extremely low wear rate  $(\sim 4.4 \times 10^{-7} \,\mathrm{mm}^3 \cdot \mathrm{N}^{-1} \cdot \mathrm{m}^{-1})$  in 3.5 wt% NaCl solution [13]. Wang et al. [14] proved that the heat treatment at 300°C would obviously enhance the wear resistance of (TiV-CrAlMo)N coating. And the thermal stability of coating must be considered because of the transient temperature generated during the wear process [15]. From the literature, the HEA and C containing HEA exhibit a good thermal stability [16,17]. As aforementioned, the introduction of non-metallic elements (C or N) and heat treatment can effectively improve the tribo-corrosion resistance of the coating. However, there is a lack of systematic study about the effect of C/N and heat treatment simultaneously on the mechanical property and tribo-corrosion resistance of HEA coating.

From the previous literature on the VAlTiCrCu [18], VAlTiCrMo [19], and VAlTiCrSi [20] coating, remarkable results on tribo-corrosion or corrosion resistance were reported. Therefore, V, Al, Ti, Mo, and Si were selected as the principal element of the HEA coating. In this work, to investigate the effect of C and heat on the microstructure, mechanical, and tribo-corrosion properties, 20 and 40 at% of C were introduced into the HEA coatings by magnetron sputtering. The hardness and elastic modulus of the asdeposited and heat-treated coating were tested at the ambient temperature. The friction and corrosion experiments were operated simultaneously in 3.5 wt% NaCl solution.

## 2 Experiment

#### 2.1 HEA coatings preparation

The HEA coatings were deposited on 304 stainless steel and Si (100) substrates by a Hauzer Flexicoat 850 DC magnetron sputtering system. The rectangular metal blocks with target sizes of 125 mm × 10 mm × 12 mm, that is high purity (≥99 %) V, Al, Ti, Mo, and Si, were stacked in the vertical direction in the order of V–Al–Ti–Mo–Si from top to bottom, forming a total of 12 target cycles. A monolithic graphite target (600 mm × 125 mm × 12 mm) is utilized to introduce carbon into the coatings. Before fixing the substrates into tunable sample racket, the substrates were

subsequently ultrasonically cleaned with acetone and ethanol for 30 min, respectively. When the chamber vacuum pressure value is lower than  $1.0\times10^{-4}$  Pa, the targets were etched by argon ions bombardment to remove the oxides and contaminants. During the deposition process, the sputtering power of V–Al–Ti–Mo–Si composite target was 2,000 W, the graphite targets were 0, 1,000, and 2,500 W, the substrate bias was –50 V, the rotation speed of sample racket was 2 rpm, and the substrate temperature was around  $100^{\circ}$ C. The abovementioned parameters were maintained for 7 h to prepare the VAlTiMoSi and VAlTiMoSiC<sub>x</sub> coatings.

#### 2.2 Heat treatment of the HEA coatings

The HEA coatings on 304 stainless steel were put into a vacuum tube furnace. Prior to heat treatment, the residual oxygen in the quartz tube was extracted. According to the result of the phase transformation, 700°C was selected as the temperature of heat treatment, and argon gas was used as a protective gas. The heating rate is 10 °C·min<sup>-1</sup> and the holding time is 1h at 700°C, then all the samples were cooled to ambient temperature in the furnace.

#### 2.3 Mechanical and tribo-corrosion tests

The Nanoidenter (G200, MTS) was conducted to characterize the mechanical properties of the coatings at room temperature in a mode of fixed 1,000 nm depth. The six test points for a sample ensure the convince data. The hardness and elastic modulus were calculated by Nanosuit software that embedded the method of Oliver-Pharr. The tribological properties of the HEA coatings were performed on a friction tester (Rtec MFT5000) in 3.5 wt% NaCl solution, simultaneously, the corrosion resistance of the coatings was measured by a Modulab analyzer. Three-electrode electrochemical method was used to obtain the open circuit potential (OCP) result, the Ag/AgCl worked as reference electrode, a platinum wire as a counter electrode, and the HEA coatings as working electrode. With regard to the obtained friction curve, the applied load is 1 N, grinding pair is Si<sub>3</sub>N<sub>4</sub> ball with a diameter of 6 mm, the sliding frequency is 1 Hz, and the sliding speed is 1 cm·s<sup>-1</sup>. The wear rate was calculated using the following formula:

$$w = \frac{Sl}{FL},\tag{1}$$

where S is the area of the wear scar, l is the length of grinding track (5 mm), F is the applied load, and L is the total sliding length (18 m). The detailed experimental process can be referred to in the literature [18].

#### 2.4 Characterization methods

The surface and cross-sectional morphologies of the as-prepared and heat-treated coatings were analyzed by scanning electron microscope (SEM; Verios G4 UC). The wear scar morphologies of the tested coatings were observed by Verios G4 UC, likewise. To precisely collect the chemical composition of the as-deposited coatings, the glow-discharge optical emission spectrometry (GDA 750HP) was used. The crystal structure was detected by X-ray diffractometer (XRD; D8 Advance Davinci) with Cu-Ka source ( $\lambda$  = 0.154 nm), and the scanning angle ranged from 10° to 90°. The profile of the wear scar that is perpendicular to the wear scar direction was obtained by a Profilometer (ASTQ, America). To analyze the effect of the heat treatment on the structure and elemental distribution, transmission electron microscope (TEM; Talos F200x) was operated to characterize the cross-sectional morphology and mapping. Additionally, the sample was pretreated by focused ion beam (Carl Zeiss Auriga).

### 3 Results and discussion

## 3.1 Microstructure and morphologies of the coatings

Table 1 gives the chemical composition of the as-deposited coating. It indicates that the atomic percentage of elemental constant covers the range from 5 to 35 at% of the HEA. The difference in sputtering yield of the target caused various relative atomic percent [21]. The C content in the coatings increased with the increased sputtering power. For the purpose of concise description, the as-deposited

Table 1: Chemical composition of the as-prepared HEA coatings (at%)

Sample	٧	Al	Ti	Мо	Si	С
VAlTiMoSi	15.90	25.77	19.12	10.38	28.83	_
(VAlTiMoSi) <sub>80</sub> C <sub>20</sub>	13.74	16.67	14.38	10.87	20.94	23.36
(VAlTiMoSi) <sub>60</sub> C <sub>40</sub>	10.04	13.42	11.10	10.79	14.67	39.98

HEA coatings were named as VAlTiMoSi, (VAlTiMoSi)<sub>80</sub>C<sub>20</sub>, and (VAlTiMoSi)<sub>60</sub>C<sub>40</sub> according to the atomic percentage of C.

Figure 1 illustrates XRD patterns of the as-deposited and heat-treated HEA coatings. The peak located at 43.7°, 50.8°, and 74.7° corresponds to the 304 stainless steel. The as-deposited VAlTiMoSi HEA coating and carbonized VAl-TiMoSi HEA coating exhibited an amorphous structure as shown in Figure 1(a). The introduction of carbon into the coating further promoted the amorphization of the coating. Considering that the XRD diffraction peak position of the amorphous phase overlaps with the BCC phase, the microstructure of the coatings will be further characterized later [22]. For the heat-treated coatings, it can be obviously observed from Figure 1(b) that heat treatment has a positive effect on crystallization of the HEA coatings on 304 stainless steel. After heat treatment, the crystallization of VAlTiMoSi coating was promoted, resulting in the formation of Mo<sub>3</sub>Si, Ti<sub>5</sub>Si<sub>4</sub>, TiSi<sub>2</sub>, and AlV<sub>3</sub>. Comparing the XRD patterns of the heat-treated coatings, higher C content inhibited the formation of the Mo<sub>2</sub>C and Ti<sub>5</sub>Si<sub>4</sub>.

The microstructure of the VAlTiMoSi, (VAlTiMoSi)<sub>80</sub>C<sub>20</sub>, and (VAlTiMoSi)<sub>60</sub>C<sub>40</sub> coatings is presented in Figure 2. As shown in Figure 2(a), all the as-deposited coatings showed a smooth and compact surface morphology. The introduction of C has minimal effect on the surface morphology of the VAlTiMoSi coating. And the thickness of the VAlTiMoSi, VAl-TiMoSi, and VAlTiMoSi coatings was 2.89, 2.29, and 2.65 μm, respectively. The cross-sectional structure showed a columnar shape, which is a typical morphology for magnetic sputtering coatings [23,24]. For the heat-treated HEA coatings, white and small particle in SEM view existed in all the heat-treated HEA coatings. Comparing with the as-deposited coatings, the grain size of the heat-treated coatings became larger. Additionally, the thermal effect has a significant effect on the grain growth of the C-included HEA coatings [25]. A noticeable difference can also be found on the surface morphology. The number of the white and large grain was less and more for VAlTiMoSi, VAlTiMoSi, and VAlTiMoSi coatings, respectively. From a rough statistical result of the crystal cluster size, the size of asdeposited coatings was in the range from 50 to 110 nm, and larger size ranged from 120 to 240 nm and can be found for annealed coatings. The thickness of the heattreated coatings was 2.73, 3.38, 3.22 µm, respectively.

To further analyze the effect of carbon and heat treatment on the microstructure of the coatings from a highresolution view, the TEM result of the as-deposited and heat-treated HEA coatings is shown in Figures 3 and 4, respectively. As shown in Figure 3, the compact and columnar cross-sectional morphologies of the as4 — Zhengyi Fu et al. DE GRUYTER

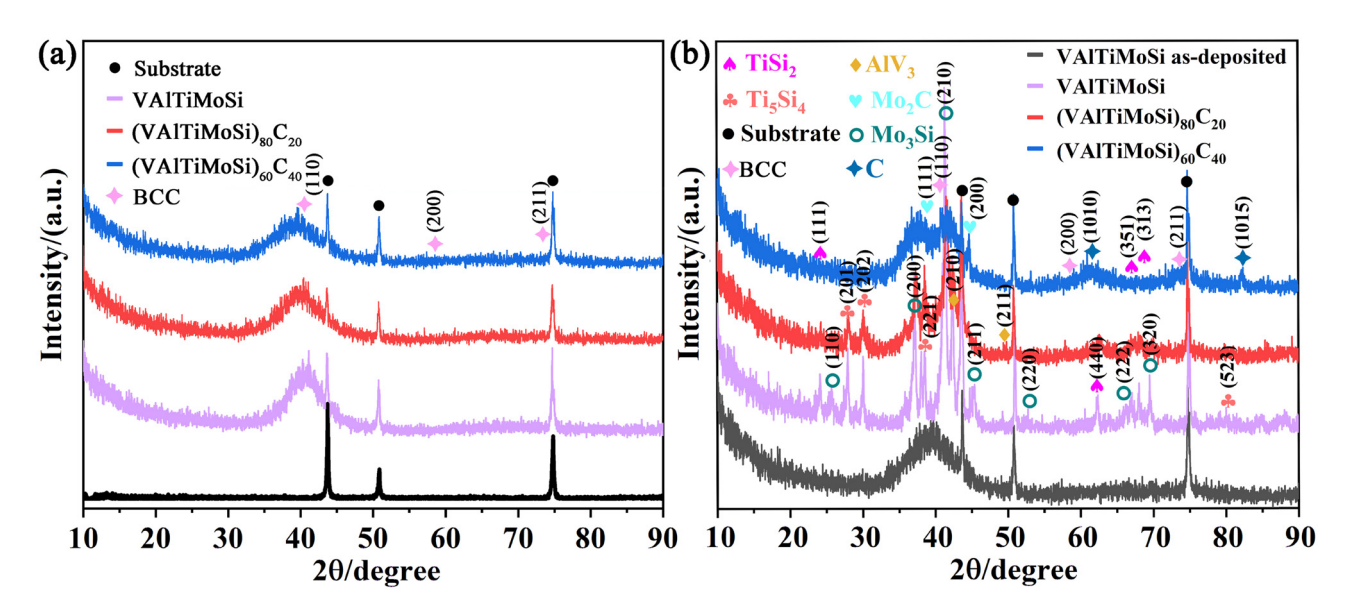
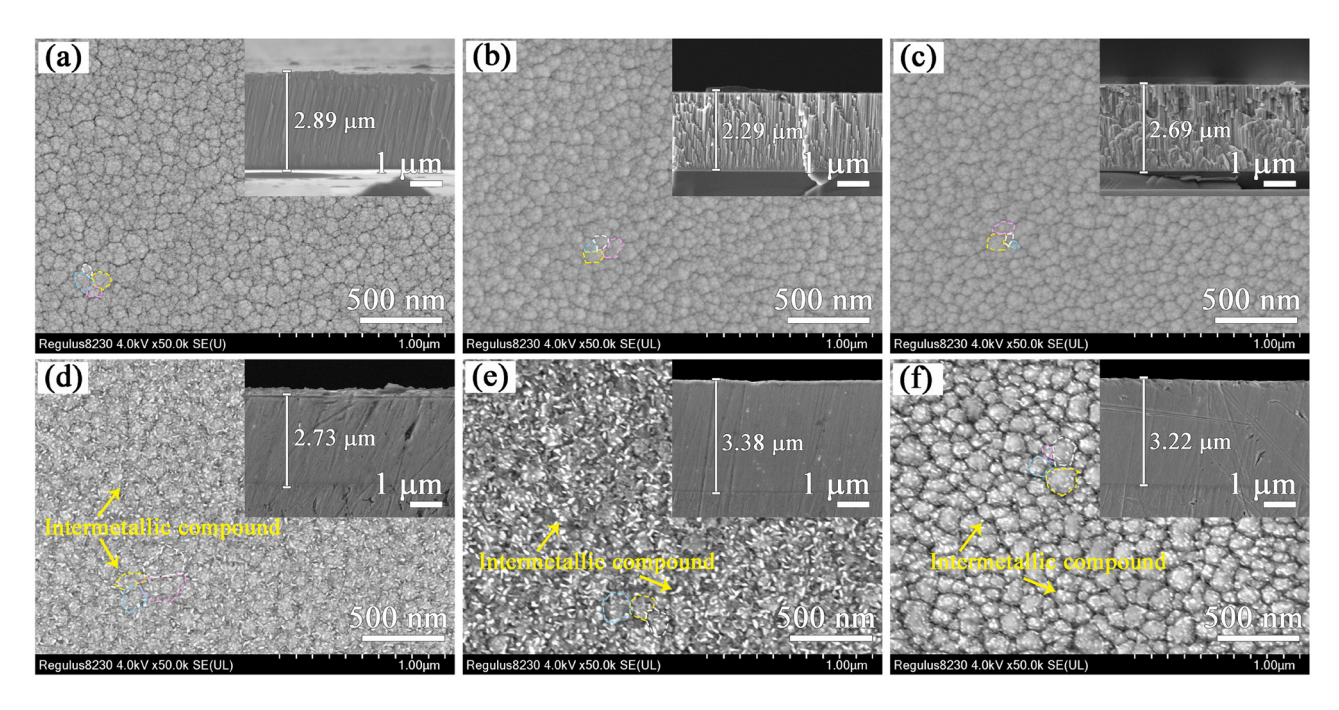


Figure 1: XRD patterns of the (a) as-prepared and (b) heat-treated HEA coatings.



**Figure 2:** Surface and cross-sectional morphologies of the HEA coatings before heat treatment: (a) VAlTiMoSi, (b) (VAlTiMoSi)<sub>80</sub>C<sub>20</sub>, (c) (VAlTiMoSi)<sub>60</sub>C<sub>40</sub>, and after annealing at 700°C (d) VAlTiMoSi, (e) (VAlTiMoSi)<sub>60</sub>C<sub>20</sub>, (f) (VAlTiMoSi)<sub>60</sub>C<sub>40</sub>.

deposited coatings can be obviously observed. (VAlTi-MoSi) $_{80}$ C $_{20}$  coating almost has the same size as the columnar structure with VAlTiMoSi coating. However, higher content of C may promote a little coarser columnar structure as shown in Figure 3(c). From the corresponding elemental mapping of the coatings, all the as-deposited HEA coatings have a uniform element distribution. Furthermore, combined with XRD patterns in Figure 1(a) and corresponded

selected area electron diffraction (SAED) patterns in Figure 3, it can be seen that all the coatings are mainly composed of BCC polycrystalline and amorphous.

For the heat-treated HEA coatings, the columnar structure of the VAlTiMoSi disappeared and formed large size grains as shown in Figure 4. Contrarily, the thermal effect is unfavorable in modification of the columnar structure of the C-included HEA coatings, and the compact and

**DE GRUYTER** 

500 nm

Figure 3: TEM images of the cross-sectional morphologies, corresponding elemental mapping, and SAED patterns of the as-deposited coatings: (a) VAlTiMoSi, (b) (VAlTiMoSi) $_{80}$ C $_{20}$ , and (c) (VAlTiMoSi) $_{60}$ C $_{40}$ .

6 — Zhengyi Fu et al. DE GRUYTER

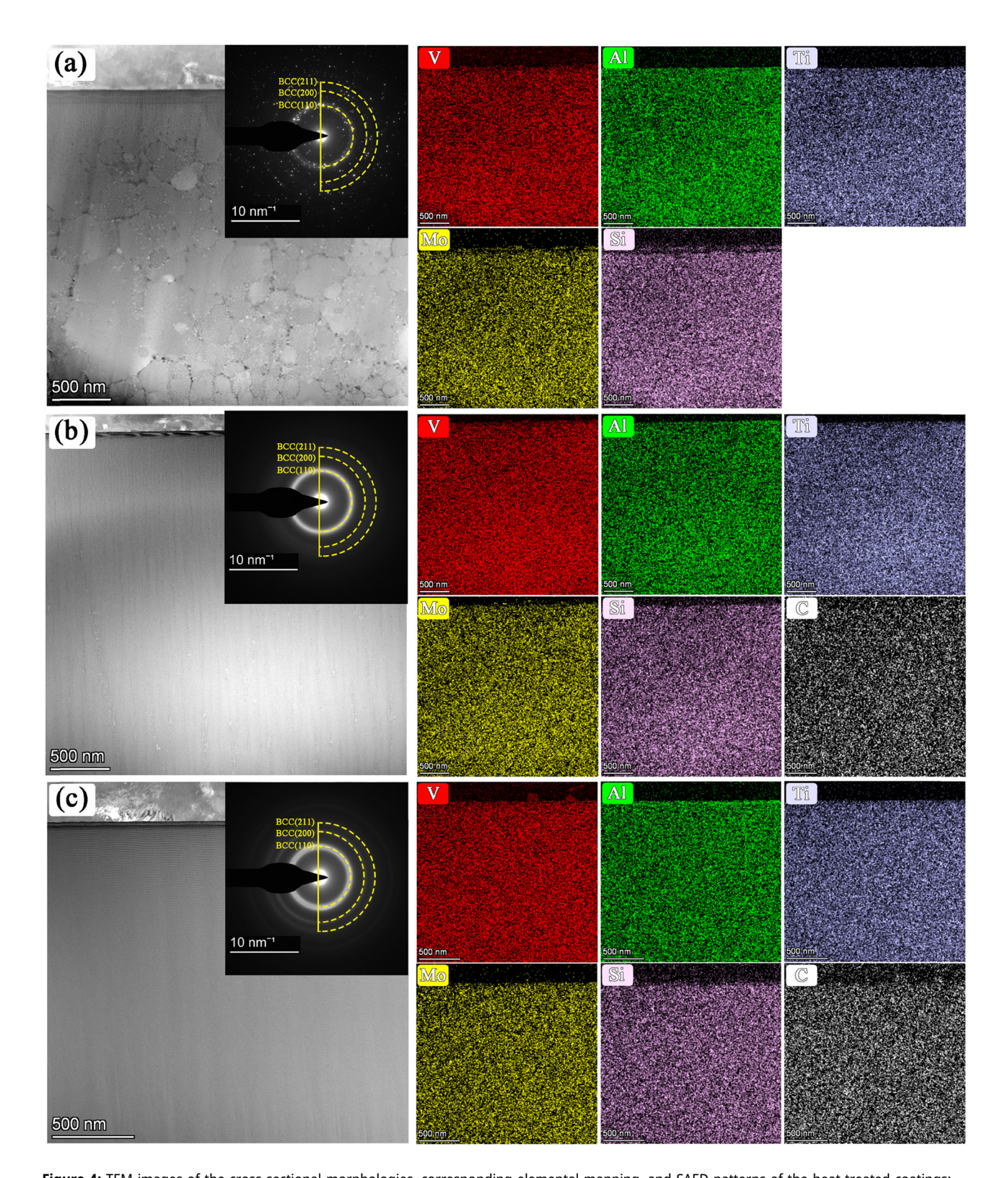


**Figure 4:** TEM images of the cross-sectional morphologies, corresponding elemental mapping, and SAED patterns of the heat-treated coatings: (a) VAlTiMoSi) $_{80}$ C $_{20}$ , and (c) (VAlTiMoSi) $_{60}$ C $_{40}$ .

columnar cross-sectional morphologies were almost the same as the as-prepared C-included coatings, correspondingly. As for the elemental mappings, there is a slice of element segregation in the VAlTiMoSi coating. (VAlTiMoSi) $_{60}$ C $_{20}$  and (VAlTiMoSi) $_{60}$ C $_{40}$  coatings have outstanding ability in anti-segregation. From the corresponding SAED patterns, the crystallization degree of C-included coatings was lower than that of VAlTiMoSi coating, which is consistent with the XRD results in Figure 1(b).

# 3.2 Mechanical and tribo-corrosion properties

The hardness and elastic modulus of the as-deposited and heat-treated HEA coatings are presented in Figure 5. As can be seen in Figure 5(a), the hardness and elastic modulus of VAITiMoSi coating were 10.4 and 200.1 GPa, respectively. The hardness of C-included HEA coatings was higher than VAITiMoSi coating, and the hardness and elastic

modulus of the (VAlTiMoSi)<sub>80</sub>C<sub>20</sub> coating were 12.6 and 215.6 GPa, respectively, because of the solid-solution strengthening of C. However, higher C content coating is inferior in the mechanical property compared with (VAl-TiMoSi)<sub>80</sub>C<sub>20</sub> coating, which is mainly attributed to the increased content of amorphous carbon [26]. For the heat-treated HEA coatings, the mechanical properties of all the coatings significantly improved, as shown in Figure 5(b). The VAlTiMoSi and (VAlTiMoSi)<sub>60</sub>C<sub>40</sub> coatings shared almost the same hardness, around 20.1 and 19.6 GPa, respectively. And the hardness of the heat-treated VAlTi-MoSi coating is almost twice that of the as-prepared VAlTiMoSi coating. Comparing Figure 1(a) and (b), the intermetallic compounds Mo<sub>3</sub>Si, Mo<sub>2</sub>C, AlV<sub>3</sub>, etc., contributed to the higher hardness. It is widely shared that the value of H/E is closely related to the damage resistance and elastic strain capacity of the coating, and the ratio of  $H^3/E^2$  can represent the ability of the film to resist crack initiation and propagation to a certain extent [27,28]. Consequently, the higher ratio of H/E and H<sup>3</sup>/E<sup>2</sup> means the higher wear resistance [29]. The (VAlTiMoSi)<sub>60</sub>C<sub>40</sub> coating

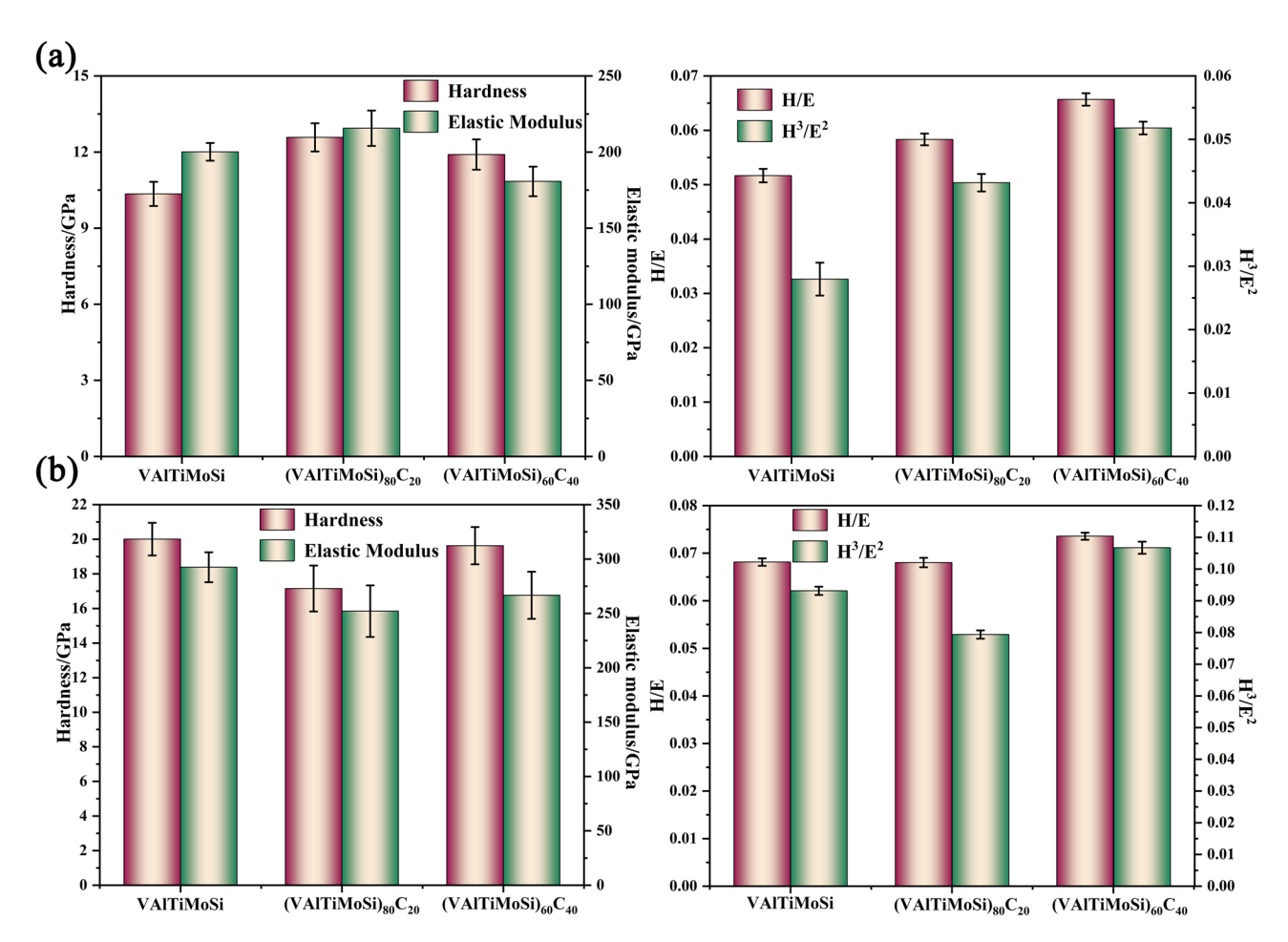


Figure 5: Hardness and elastic modulus, the ratio of H/E and H<sup>3</sup>/E<sup>2</sup> of the HEA coatings: (a) as-prepared coatings and (b) heat-treated coatings.

8 — Zhengyi Fu et al. DE GRUYTER

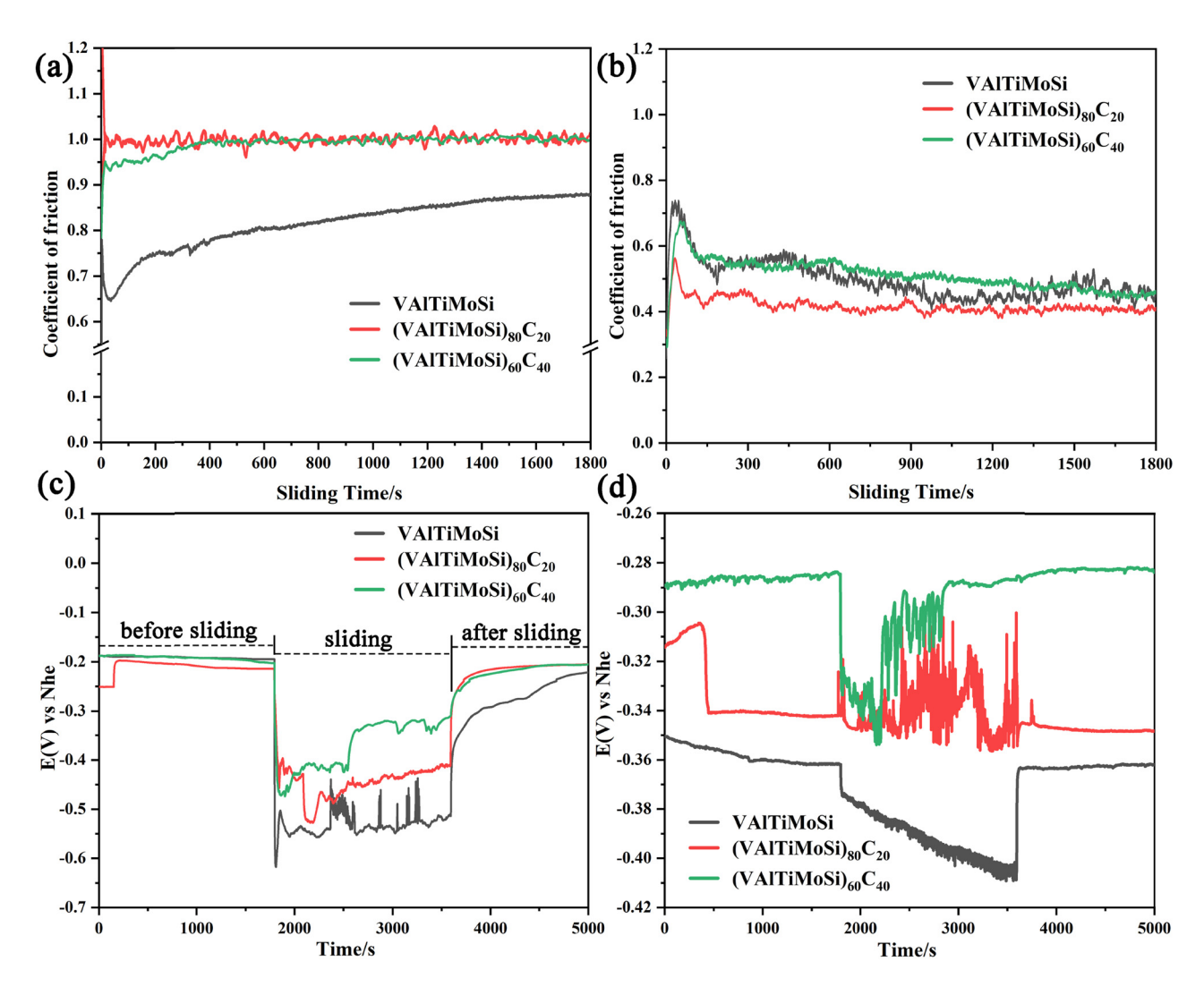


Figure 6: COF and OCP curves of the HEA coatings tested in 3.5 wt% NaCl solution: (a and c) as-deposited coatings and (b and d) heat-treated coatings.

gained the highest H/E and  $\mathrm{H}^3/\mathrm{E}^2$  value when compared with as-deposited or heat-treated VAlTiMoSi and (VAlTiMoSi)<sub>80</sub>C<sub>20</sub> coatings, respectively. And the heat treatment promoted the wear resistance, since the value of H/E and  $\mathrm{H}^3/\mathrm{E}^2$  were higher than as-deposited coatings.

The friction curve in a reciprocating friction mode of the coatings is shown in Figure 6. For the as-prepared coatings, the coefficient of friction (COF) of the VAlTiMoSi coating was lower than C-included coatings. The average COF of the VAlTiMoSi coating was 0.79, which is higher than most of the HEA coatings [7,30,31]. The higher C content did not reduce the COF of the (VAlTiMoSi) $_{60}$ C $_{40}$  coating, the COF of (VAlTiMoSi) $_{80}$ C $_{20}$  and (VAlTiMoSi) $_{60}$ C $_{40}$  coating was approximately equal. However, the heat-treated HEA coatings had a relative lower COF than as-prepared coatings. The average COF of all the heat-treated coatings was not higher than 0.6, and the lowest average COF was 0.42, belonging to the (VAlTiMoSi) $_{80}$ C $_{20}$  coating.

The OCP evolution of the working electrode contributes to obtain the qualitative information of electrochemical state during the tribo-corrosion test. The OCPs of the tested HEA coatings, during, and after the tribo-corrosion tested in 3.5 wt% NaCl solution are shown in Figure 6(c) and (d). In terms of static corrosion resistance, the OCP value of the as-deposited VAlTiMoSi and (VAlTiMoSi)80C20 coatings was relatively higher than (VAlTiMoSi)<sub>60</sub>C<sub>40</sub> coating. However, the OCP value of the heat-treated VAlTiMoSi coating is the lowest, which means that thermal effect failed to enhance VAlTiMoSi coating in static corrosion resistance. Upon commencing the friction test, it is observed that all the coatings exhibited a significant negative deviation in their OCP curves. This deviation is derived from the mechanical destruction of the passive film. During the friction process, the OCP curves of the coating fluctuate. The fluctuation can be mainly attributed to the formation and destruction of the passive film during the reciprocating motion of the grinding

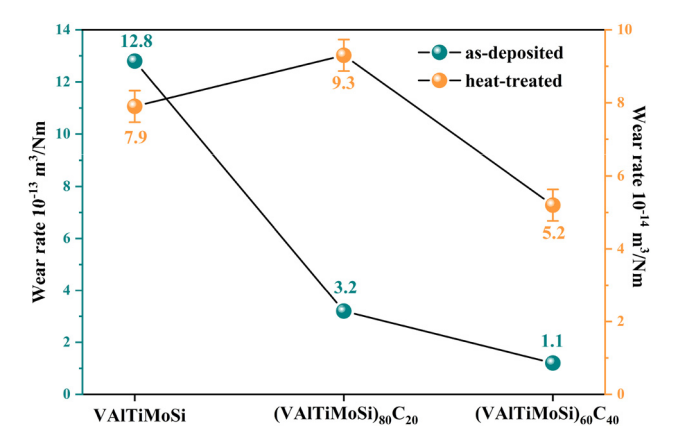


Figure 7: Wear rate of the tested HEA coatings.

pair. After the friction test, the OCP value almost returned back to its original state, indicating the reformation of the complete passive film. Additionally, as shown in Figure 6(d), the C-included coatings had a better formation ability of the passive film. And the complete passive film of the (VAlTi-MoSi) $_{60}C_{40}$  coating has been formed before the end of the friction process.

The wear rate is an evaluation index of wear duration, and the wear rate of the coatings is depicted in Figure 7. As

shown in Figure 7(a), the wear rate of the as-prepared (VAlTiMoSi) $_{80}$ C $_{20}$  and (VAlTiMoSi) $_{60}$ C $_{40}$  coatings was lower than  $3.5 \times 10^{-13}$  m $^3 \cdot \text{Nm}^{-1}$ , while the VAlTiMoSi coating was higher than  $1.0 \times 10^{-12}$  m $^3 \cdot \text{Nm}^{-1}$ . Introducing C into the HEA coating significantly improved the wear resistance. Comparing with the as-prepared coatings, the wear resistance of the heat-treated coating improved constructively. The wear rate of the heat-treated VAlTiMoSi coating reduced by more than one order of magnitude, and the (VAlTiMoSi) $_{60}$ C $_{40}$  coating had the lowest wear rate, *i.e.*,  $5.2 \times 10^{-14}$  m $^3 \cdot \text{Nm}^{-1}$ . Particularly, the as-prepared and heat-treated (VAlTiMoSi) $_{60}$ C $_{40}$  coating obtained the lowest wear rate among the tested coatings.

To analyze the wear mechanism of HEA coatings, the morphologies of the wear track were collected. As can be seen in Figure 8(a), furrows obviously distributed along the sliding direction, which means abrasive wear dominated in the wear track of the as-deposited coatings. Especially, for the VAlTiMoSi and (VAlTiMoSi) $_{80}$ C $_{20}$  coatings, delamination on the edge of the wear track appeared, it indicates that delamination wear also existed, that is why these two kinds of coatings had higher wear rate than (VAlTiMoSi) $_{60}$ C $_{40}$  coating. After heat treatment, the plowing effect of VAlTiMoSi and (VAlTiMoSi) $_{60}$ C $_{40}$  coatings decreased

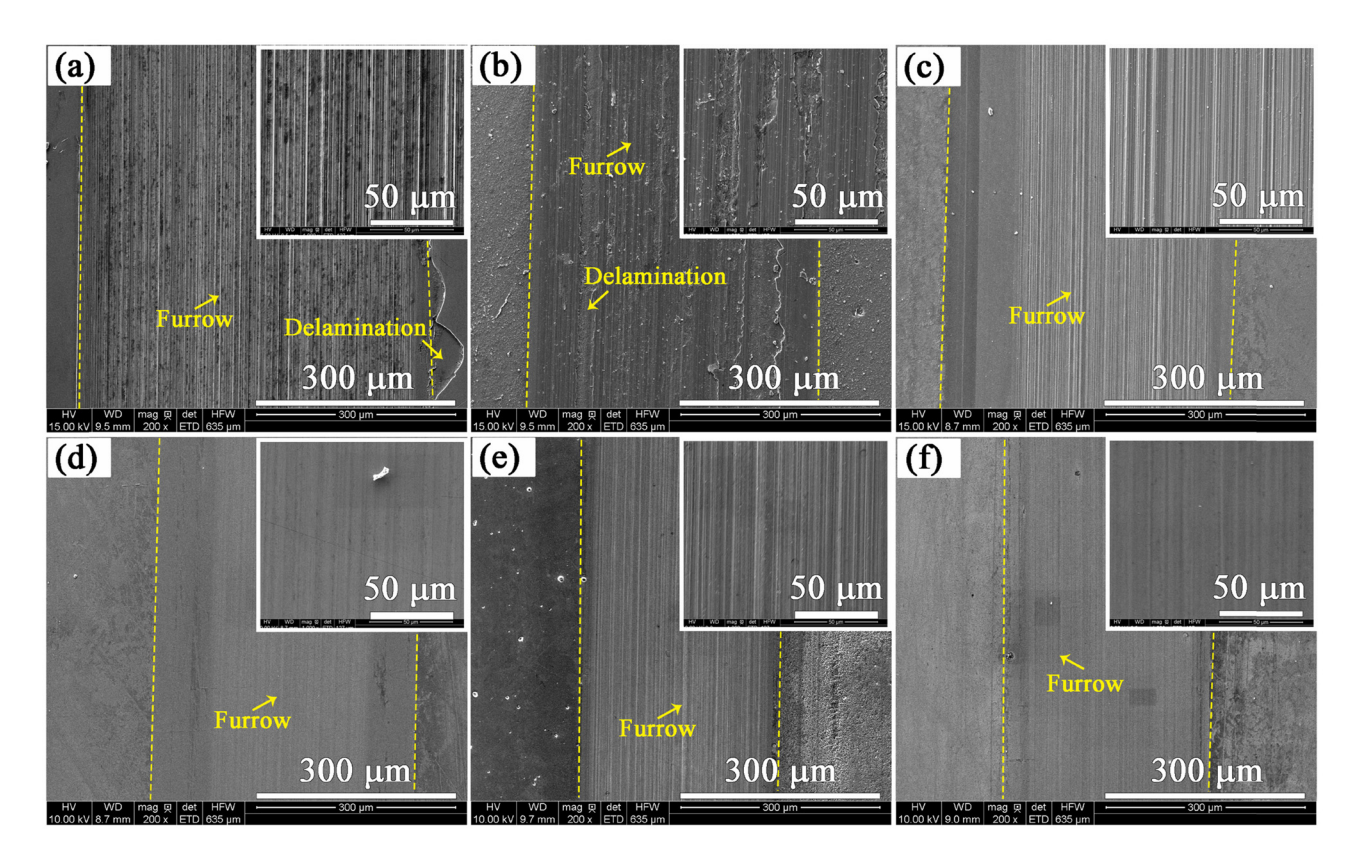


Figure 8: Morphologies of the wear track of the tested coatings: (a and d) VAlTiMoSi, (b and e) (VAlTiMoSi) $_{80}$ C $_{20}$ , and (c and f) (VAlTiMoSi) $_{60}$ C $_{40}$ .

significantly, and the delamination of VAlTiMoSi and (VAlTiMoSi) $_{80}$ C $_{20}$  coatings disappeared. Additionally, known from the wear track marked by yellow dash lines, the width of wear track of heat-treated coatings is narrower than as-deposited coatings. Therefore, the wear rate of all the heat-treated HEA coatings decreased. However, the furrows in the wear track of (VAlTiMoSi) $_{80}$ C $_{20}$  coating were conspicuous, which can elaborate the higher wear rate compared with VAlTiMoSi coating. Abrasive wear is the main wear mechanism of these heat-treated coatings. Considering the mechanical and tribo-corrosion properties, the heat-treated (VAlTiMoSi) $_{60}$ C $_{40}$  coating has the best application prospect.

# 3.3 Effect of C and heat treatment on the HEA coatings

For the as-deposited coatings, a slice of C enhanced the mechanical properties of the HEA coating by solid-solution strengthening, and the excessive C cannot further improve the hardness of the coating due to the formation of amorphous carbon. Known from the XRD patterns of heat-treated coatings, that the C inhibited the formation of Si-containing intermetallic compounds (Mo<sub>3</sub>Si and Ti<sub>5</sub>Si<sub>4</sub>), and C replaced Si to form Mo<sub>2</sub>C.

Heat treatment released the internal stress of the coatings and induced the existence of intermetallic compounds. After heat treatment, the bigger grain size of the (VAlTiMoSi) $_{60}$ C $_{40}$  coating reduced the number of grain boundaries, which contributed to the corrosion resistance. Comparing the OCPs of the heat-treated coatings, unlike Mo $_2$ C, Mo $_3$ Si was hardly able to promote the formation of passive film.

#### 4 Conclusions

To address the effect of C and heat treatment on the microstructure, mechanical, and tribo-corrosion properties of HEA coating, the VAlTiMoSi, (VAlTiMoSi) $_{80}$ C $_{20}$ , and (VAlTiMoSi) $_{60}$ C $_{40}$  coatings were successfully prepared by DC magnetron sputtering.

All the as-deposited coatings were composed of BCC and amorphous phases. Heat treatment significantly improved the mechanical and tribo-corrosion properties of the HEA coatings. The hardness of the heat-treated coatings was increased by 36–93%, and the values of H/E and  $\rm H^3/E^2$  of (VAlTiMoSi) $_{60}\rm C_{40}$  coating were up to 0.07 and 0.11, respectively. In particular, the wear rate of the heat-treated

VAlTiMoSi coating reduced by more than one order of magnitude compared with as-deposited VAlTiMoSi coating. The COF of the heat-treated coatings is lower than 0.6. Abrasive wear dominated the wear mechanism after heat treatment. The improvement in tribo-corrosion resistance and mechanical properties of the coatings is mostly due to the reduction of residual stress and the generation of intermetallic compounds.

**Acknowledgments:** The authors thank the teachers, leaders and colleagues who provided the necessary support for the implementation of the project, in addition to the anonymous reviewers for their productive suggestions for improving the article.

Funding information: The authors state no funding involved.

Author contributions: Zhengyi Fu: conceptualization, methodology, formal analysis, writing – original draft, data curation, visualization, validation; Sansan Ding: data curation, visualization, validation, supervision. Aiqin Tian: methodology; Dawei Chen: investigation; Xu Chen: methodology, supervision; Huaqiang Lin: methodology, supervision; Zhongwen Li: methodology; Xiaohong Sun: methodology, supervision; Xiangjian Meng: investigation, methodology; Wei Zhou: conceptualization, supervision, funding acquisition. All authors have accepted the responsibility for the entire content of this manuscript and approved its submission.

**Conflict of interest:** The authors state no conflict of interest.

#### References

- [1] Robert, J. K. Marine wear and tribocorrosion. Wear, Vol. 376–377, 2017, pp. 893–910.
- [2] Ma, F. L., J. L. Li, Z. X. Zeng, and Y. M. Gao. Structural, mechanical and tribocorrosion behaviour in artificial seawater of CrN/AlN nano-multilayer coatings on F690 steel substrates. *Applied Surface Science*, Vol. 428, 2018, pp. 404–414.
- [3] Li, H., L. L. Liu, P. Guo, L. L. Sun, J. Wei, Y. R. Liu, et al. Long-term tribocorrosion resistance and failure tolerance of multilayer carbon-based coatings. *Friction*, Vol. 10, 2022, pp. 1707–1721.
- [4] Chen, Q., Y. Z. Cao, Z. W. Xie, T. Chen, Y. Y. Wan, H. Wang, et al. Tribocorrosion behaviors of CrN coating in 3.5 wt% NaCl solution. *Thin Solid Films*, Vol. 622, 2017, pp. 41–47.
- [5] Li, B., C. Li, Y. M. Gao, H. J. Guo, Q. L. Zheng, Y. C. Kang, et al. Influence of heat treatment on corrosion-wear behavior of Nibased coating in artificial seawater. *Journal of Materials Engineering* and Performance, Vol. 28, 2019, pp. 7828–7834.
- [6] Wang, G. Y., J. Xu, Y. H. Chen, Y. J. Zhao, Z. H. Xie, and P. R. Munroe. Assessment of the tribocorrosion performance of a (TiZrNbTaMo)C

- refractory high entropy alloy carbide coating in a marine environment. Journal of Alloys and Compounds, Vol. 965, 2023, id. 171342.
- [7] Wen, X., X. F. Cui, G. Jin, Y. F. Liu, Y. Zhang, X. R. Zhang, et al. Corrosion and tribo-corrosion behaviors of nano-lamellar Ni<sub>1.5</sub>CrCoFe<sub>0.5</sub>Mo<sub>0.1</sub>Nb<sub>x</sub> eutectic high-entropy alloy coatings: the role of dual-phase microstructure. Corrosion Science, Vol. 201, 2022,
- Chen, B., X. M. Li, L. Y. Tian, H. Y. Jia, H. Li, and Y. Li. The CrFeNbTiMo<sub>x</sub> refractory high-entropy alloy coatings prepared on the 40Cr by laser cladding. Journal of Alloys and Compounds, Vol. 966, 2023, id. 171630.
- Jiang, D., H. Z. Cui, X. F. Zhao, H. Chen, G. L. Ma, and X. J. Song. Synergistic improvement of wear and corrosion resistance of CoCrNiMoCB coatings obtained by laser cladding: role of Mo concentration. Materials & Design, Vol. 219, 2022, id. 110751.
- [10] Niu, D. W., C. X. Zhang, X. D. Sui, X. L. Lu, X. Zhang, C. Wang, et al. Microstructure, mechanical properties and tribo-corrosion mechanism of (CrNbTiAlVMo)<sub>x</sub>N<sub>1-x</sub> coated 316 L stainless steel in 3.5 wt% NaCl solution. Tribology International, Vol. 173, 2022, id. 107638.
- [11] Miao, J. W., H. W. Yao, J. Wang, Y. P. Lu, T. M. Wang, and T. J. Li. Surface modification for AlCoCrFeNi<sub>2.1</sub> eutectic high-entropy alloy via laser remelting technology and subsequent aging heat treatment. Journal of Alloys and Compounds, Vol. 894, 2022, id. 162380.
- Niu, D. W., X. Zhang, X. D. Sui, Z. Q. Shi, X. L. Lu, C. Wang, et al. Tailoring the tribo-corrosion response of (CrNbTiAlV)C<sub>x</sub>N<sub>y</sub> coatings by controlling carbon content. Tribology International, Vol. 179, 2023, id. 108179.
- [13] Zhang, C. X., X. L. Lu, H. B. Zhou, Y. F. Wang, X. D. Sui, Z. Q. Shi, et al. Construction of a compact nanocrystal structure for (CrNbTiAlV)N<sub>x</sub> high-entropy nitride films to improve the tribo-corrosion performance. Surface and Coatings Technology, Vol. 429, 2022, id. 127921.
- [14] Wang, Z., F. H. Chen, Y. H. Dong, Z. B. Cai, P. Zhang, J. Chen, et al. Effect of heat-treatment time on microstructure and tribological behavior of (TiVCrAlMo)N high-entropy alloy films. Surface and Coatings Technology, Vol. 443, 2022, id. 128618.
- [15] Li, S. and A. Anisetti. On the flash temperature of gear contacts under the tribo-dynamic condition. Tribology International, Vol. 97, 2016, pp. 6-13.
- [16] Jain, H., Y. Shadangi, D. Chakravarty, K. Chattopadhyay, A. K. Dubey, and N. K. Mukhopadhyay. Low-density Fe<sub>40</sub>Mn<sub>19</sub>Ni<sub>15</sub>Al<sub>15</sub>Si<sub>10</sub>C<sub>1</sub> high entropy steel processed by mechanical alloying and spark plasma sintering: phase evolution, microstructure and mechanical properties. Materials Science and Engineering: A, Vol. 869, 2023, id. 144776.
- [17] Jain, H., Y. Shadangi, D. Chakravarty, D. A. Kumar, and N. K. Mukhopadhyay. High entropy steel processed through mechanical alloying and spark plasma sintering: alloying behaviour, thermal stability and mechanical properties. Materials Science and Engineering: A, Vol. 856, 2022, id. 144029.
- Chen, S. Y., Z. B. Cai, Z. X. Lu, J. B. Pu, R. Chen, S. J. Zheng, et al. Tribo-corrosion behavior of VAlTiCrCu high-entropy alloy film. Materials Characterization, Vol. 157, 2019, id. 109887.

- [19] Chen, R., Z. B. Cai, J. B. Pu, Z. X. Lu, S. Y. Chen, S. J. Zheng, et al. Effects of nitriding on the microstructure and properties of VAlTiCrMo high-entropy alloy coatings by sputtering technique. Journal of Alloys and Compounds, Vol. 827, 2020, id. 153836.
- Zheng, S. J., Z. B. Cai, J. B. Pu, C. Zeng, and L. P. Wang. Passivation behavior of VAlTiCrSi amorphous high-entropy alloy film with a high corrosion-resistance in artificial sea water. Applied Surface Science, Vol. 542, 2021, id. 148520.
- [21] Depla, D. On the effective sputter yield during magnetron sputter deposition. Nuclear Instruments and Methods in Physics Research Section B: Beam Interactions with Materials and Atoms, Vol. 328, 2014, pp. 65-69.
- [22] Wang, X. R., Z. Q. Wang, W. S. Li, T. S. Lin, P. He, and C. H. Tong. Preparation and microstructure of CuNiTiZr medium-entropy alloy coatings on TC11 substrate via electrospark-computer numerical control deposition process. Materials Letters, Vol. 197, 2017,
- [23] Han, C. Z., D. Chen, Y. Z. Zhang, D. Xu, Y. J. Liu, E. S. Kong, et al. High potential columnar nanocrystalline AIN films deposited by RF reactive magnetron sputtering. Nano-Micro Letters, Vol. 4, 2012, pp. 40-44.
- [24] Suszko, T., W. Gulbiński, K. Załęski, G. Greczynski, J. Morgiel, and V. Lapitskaya. Nano-columnar, self-organised NiCrC/a-C:H thin films deposited by magnetron sputtering. Applied Surface Science, Vol. 591, 2022, id. 153134.
- Murdoch, H. A. and C. A. Schuh. Stability of binary nanocrystalline [25] alloys against grain growth and phase separation. Acta Materialia, Vol. 61, No. 6, 2013, pp. 2121-2132.
- Jhong, Y. S., C. W. Huang, and S. J. Lin. Effects of CH<sub>4</sub> flow ratio on [26] the structure and properties of reactively sputtered (CrNbSiTiZr)C<sub>x</sub> coatings. Materials Chemistry and Physics, Vol. 210, 2018, pp. 348-352.
- Musil, J. and M. Jirout. Toughness of hard nanostructured ceramic thin films. Surface and Coatings Technology, Vol. 201, No. 9-11, 2007, nn. 5148-5152.
- [28] Dang, C. Q., J. L. Li, Y. Wang, and J. M. Chen. Structure, mechanical and tribological properties of self-toughening TiSiN/Ag multilayer coatings on Ti6Al4V prepared by arc ion plating. Applied Surface Science, Vol. 386, 2016, pp. 224-233.
- [29] Leyland, A. and A. Matthews. On the significance of the H/E ratio in wear control: a nanocomposite coating approach to optimised tribological behaviour. Wear, Vol. 246, No. 1-2, 2000, pp. 1-11.
- [30] Fu, Y., C. Huang, C. W. Du, J. Li, C. D. Dai, H. Luo, et al. Evolution in microstructure, wear, corrosion, and tribocorrosion behavior of Mo-containing high-entropy alloy coatings fabricated by laser cladding. Corrosion Science, Vol. 191, 2021, id. 109727.
- Karakaş, M. S., A. Günen, C. Çarboğa, Y. Karaca, M. Demir, [31] Y. Altınay, et al. Microstructure, some mechanical properties and tribocorrosion wear behavior of boronized  $Al_{0.07}Co_{1.26}Cr_{1.80}Fe_{1.42}Mn_{1.35}Ni_{1.10}$  high entropy alloy. Journal of Alloys and Compounds, Vol. 886, 2021, id. 161222.